International Journal of Heat and Mass Transfer 78 (2014) 447–459

Contents lists available at ScienceDirect

International Journal of Heat and Mass Transfer

journal homepage: www.elsevier.com/locate/ijhmt

Stability of natural convection in a vertical couple stress fluid layer

B.M. Shankar [a,*], Jai Kumar [b], I.S. Shivakumara [c]

[a] Department of Mathematics, PES Institute of Technology, Bangalore 560 085, India
[b] ISRO Satellite Centre, Bangalore 560 017, India
[c] Department of Mathematics, Bangalore University, Bangalore 560 001, India

ARTICLE INFO

Article history:
Received 10 February 2014
Received in revised form 14 May 2014
Accepted 29 June 2014

Keywords:
Couple stress fluid
Natural convection
Modified Orr–Sommerfeld equation
Linear stability

ABSTRACT

The stability of buoyancy-driven parallel shear flow of a couple stress fluid confined between vertical plates is investigated by performing a classical linear stability analysis. The plates are maintained at constant but different temperatures. A modified Orr–Sommerfeld equation is derived and solved numerically using the Galerkin method with wave speed as the eigenvalue. The critical Grashof number G_c, critical wave number a_c and critical wave speed c_c are computed for wide ranges of couple stress parameter Λ_c and the Prandtl number Pr. Based on these parameters, the stability characteristics of the system are discussed in detail. The value of Prandtl number, at which the transition from stationary to travelling-wave mode takes place, increases with increasing Λ_c. The couple stress parameter shows destabilising effect on the convective flow against stationary mode, while it exhibits a dual behaviour if the instability is via travelling-wave mode. The streamlines and isotherms presented demonstrate the development of complex dynamics at the critical state.

1. Introduction

Buoyancy driven flows continued to receive the attention of researchers in both heat transfer and fluid mechanics. In recent years important industrial problems in which natural convection dominates are of major focus for analysts and experimentalists. The study of fluid motions and transport processes by buoyancy have been generally motivated by the important applications such as nuclear reactor, cooling of electronic equipments, materials processing such as solidification phenomenon, atmospheric and oceanic circulations, or in air currents rising from a cooling object, crystal growth processes, and other natural convection processes in the natural calamity (spread of fire). Cooling of electronic components by natural convection is most preferable as it is highly reliable and avoids additional power consumption to induce the flow as in the case of forced convection. The recognition of high free convection heat transfer rates in atomic reactors, electrical transformers and other engineering applications prompted many to understand and study the stability of natural convection. The main interest in the study of stability of natural convection in a fluid layer is to know when and how laminar flow breaks down, its subsequent development and its eventual transition to turbulence.

The stability of natural convection of a Newtonian viscous fluid which is confined between two parallel vertical plates maintained at constant and different temperatures provides one of the simplest cases of an interaction between buoyancy and shearing forces and has been investigated analytically, numerically and experimentally [1–9]. Instability of the base flow in such a vertical fluid layer occurs when the Grashof number becomes greater than a certain critical value. The most interesting observation is that the type of instability is determined by the magnitude of the Prandtl number Pr. For values of $Pr < 12.7$, the parallel flow undergoes a transition to a stationary multicell flow pattern when the Grashof number exceeds a critical value. This transition has been observed experimentally by Vest and Arpaci [6]. The critical disturbance modes are found to be travelling waves when $Pr > 12.7$.

Majority of the studies on the stability of natural convection in a vertical fluid layer are mainly concerned with Newtonian fluids which have a linear relationship between the shear stress and shear rate. However, fluid dynamical systems encountered in many practical problems cited above exhibit non-Newtonian behaviour. Therefore, studying the stability of natural convection considering non-Newtonian effects are quite desirable. Unlike Newtonian fluids, there are different kinds of non-Newtonian fluids and obviously they do not lend themselves to a unified treatment. In recent years, polar fluids – a class of non-Newtonian fluids have received a wider attention. These fluids deform and produce a spin field due to the microrotation of suspended particles. As far as

* Corresponding author.
E-mail address: bmshankar@pes.edu (B.M. Shankar).

http://dx.doi.org/10.1016/j.ijheatmasstransfer.2014.06.087
0017-9310/

Nomenclature

a	vertical wave number
c	wave speed
c_r	phase velocity
c_i	growth rate
$D = d/dx_1$	differential operator
$\vec{g}$	acceleration due to gravity
$G = \alpha g \beta h^4/\nu^2$	Grashof number
h	thickness of the dielectric fluid layer
p	pressure
$Pr = \nu/\kappa$	Prandtl number
$\vec{q} = (u_1, u_2, u_3)$	velocity vector
t	time
T	temperature
T_1	temperature of the left boundary
T_2	temperature of the right boundary
W_b	basic velocity
(x_1, x_2, x_3)	Cartesian co-ordinates

Greek symbols

α	thermal expansion coefficient
η	couple stress viscosity
κ	thermal diffusivity
$\Lambda_c = h\sqrt{\mu/\eta}$	couple stress parameter
μ	fluid viscosity
$\nu (= \mu/\rho_0)$	kinematic viscosity
$\psi(x_1, x_3, t)$	stream function
Ψ	amplitude of vertical component of perturbed velocity
ρ	fluid density
ρ_0	reference density at T_0
θ	amplitude of perturbed temperature

these types of non-Newtonian fluids are concerned, there are two important theories proposed by Eringen [10] and Stokes [11] and these are, respectively, referred to as micropolar fluid theory and couple stress fluid theory. The micropolar fluids take care of local effects arising from microstructure and as well as the intrinsic motions of microfluidics. The spin field due to microrotation of freely suspended particles set up an anti-symmetric stress, known as couple stress, and thus forming couple stress fluid. The couple-stress fluid theory represents the simplest generalisation of the classical viscous fluid theory that allows for polar effects and whose microstructure is mechanically significant in fluids. Moreover, the couple stress fluid model is one of the numerous models that were proposed to describe response characteristics of non-Newtonian fluids. The constitutive equations in these fluid models can be very complex and involve a number of parameters, also the resulting flow equations lead to boundary value problems in which the order of differential equations is higher than the Navier–Stokes equations and are given by Stokes [11] which allows the sustenance of couple stresses in addition to usual stresses. This fluid theory shows all the important features and effects of couple stresses and results in equations that are similar to Navier–Stokes equations. Couple-stress fluids have applications in a number of processes that occur in industry such as the extrusion of polymer fluids, solidification of liquid crystals, cooling of metallic plates in a bath, nuclear slurries, exotic lubricants and colloidal fluids, liquids containing long-chain molecules as polymeric suspensions, and lubrication, electro-rheological fluids to mention a few.

Work on the stability of natural convection in a vertical fluid layer subsequently extended to non-Newtonian fluids is concerned only with viscoelastic fluids ([12,13]). Jain and Stokes [14] studied the effect of couple stresses in fluids on the hydrodynamic stability of plane Poiseuille flow, while effect of couple stresses on thermal convective instability is analyzed by many researchers ([15–19]). Rudraiah et al. [20] investigated electrohydrodynamic stability of couple stress fluid flow in a horizontal channel occupied by a porous medium using energy method.

Nonetheless, the effect of couple stresses on the stability of natural convection in a vertical fluid layer has not received any attention in the literature despite its relevance and importance in many practical problems cited above. The intent of the present paper is to investigate this problem in which the vertical plates are maintained at constant but different temperatures. Modified Orr–Sommerfeld equations are derived and the resulting eigenvalue problem is solved numerically using the Galerkin method.

2. Mathematical formulation

The geometric arrangement of the problem is illustrated schematically in Fig. 1. We consider an incompressible couple stress fluid confined between two parallel vertical plates at $x_1 = \pm h$. The left surface is maintained at fixed temperature T_1, whereas the plate at $x_1 = h$ is maintained at fixed temperature T_2 ($>T_1$). A Cartesian coordinate system (x_1, x_2, x_3) is chosen with the origin in the middle of the vertical fluid layer, where the x_1-axis is taken perpendicular to the plates and the x_3-axis is vertically upwards, opposite in the direction to the gravity. Under the Oberbeck–Boussinesq approximation (since the temperature difference between the vertical plates is assumed to be small, the density is treated as a constant everywhere in the governing equation except in the gravitational term), we have

$$u_{i,i} = 0 \tag{1}$$

$$\rho = \rho_0\{1 - \alpha(T - T_0)\} \tag{2}$$

where u_i is the velocity vector, T is the temperature, ρ is the fluid density, α is the thermal expansion coefficient, ρ_0 is the density at reference temperature $T = T_0$ (at the middle of the channel).

The equation of motion for couple stress fluids are based on the constitutive equations which are given by Stokes [11]. The stress tensor τ_{ij} consists of symmetric and anti-symmetric parts and

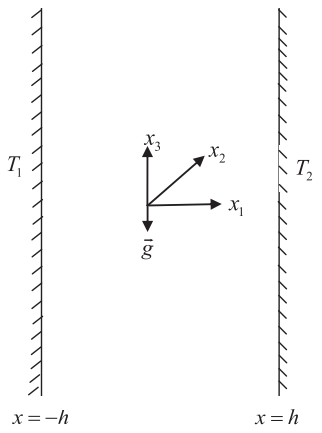

Fig. 1. Physical configuration.

the couple stress tensor M_{ij} has the linear constitutive relation. They are respectively given by

$$\tau_{ij} = \left[(-p + \lambda D_{kk})\delta_{ij} + 2\mu D_{ij}\right] - \left[2\eta W_{ij,kk} + \frac{1}{2}\varepsilon_{ijk}(\rho G_k + m_{,k})\right] \quad (3)$$

and

$$M_{ij} = \frac{1}{3}m\delta_{ij} + 4\eta\omega_{j,i} + 4\eta'\omega_{i,j} \quad (4)$$

In the above equations, p is the pressure, $D_{ij} = (u_{i,j} + u_{j,i})/2$ is the rate of deformation tensor, $W_{ij} = -(u_{i,j} - u_{j,i})/2$ is the vorticity tensor, ρG_k is the body couple vector, m is the trace of the couple stress tensor, λ and μ are the material constants having dimensions of viscosity, while η and η' are material constants having dimensions of momentum and $\omega_i = \varepsilon_{ijk}u_{j,k}/2$ is the spin vector. The equation of motion of an incompressible couple stress fluid in the presence of body force and in the absence of body couples is given by

$$\rho_0(u_{i,t} + u_j u_{i,j}) = -p_{,i} + \rho g\delta_{i3} + \mu u_{i,jj} - \eta\, u_{i,jjkk} \quad (5)$$

where g is the gravitational acceleration and δ_{ij} is the Kronecker delta symbol.

The equation of energy is

$$\rho_0 c_v(T_{,t} + u_j T_{,j}) = kT_{,jj} \quad (6)$$

where k is the thermal conductivity and c_v is the specific heat at constant volume.

3. Basic state

The basic state is a fully developed, unidirectional, steady, and laminar flow. Thus,

$$u_i = W_b(x_1)\delta_{i3}, \quad p = p_b(x_3), \quad T = T_b(x_1), \quad \rho = \rho_b(x_1) \quad (7)$$

where the subscript b denotes the basic state. Under this circumstance, the basic state solution is found to be

$$T_b - T_0 = \beta x_1/2; \ \beta = \Delta T/h \quad (8a, b)$$

$$\rho_b = \rho_0\left(1 - \frac{\alpha\beta x_1}{2}\right) \quad (9)$$

Substituting Eq. (7), in Eq. (5), we obtain

$$\eta\frac{d^4W_b}{dx_1^4} - \mu\frac{d^2W_b}{dx_1^2} - \frac{\alpha\beta\rho_0 g}{2}x_1 = 0 \quad (10)$$

with boundary conditions

$$W_b = 0 = \frac{d^2W_b}{dx_1^2} \quad \text{at } x_1 = \pm h \quad (11)$$

Solving Eq. (10) subject to the boundary conditions (11), we obtain

$$W_b = \frac{\alpha g\beta}{12\mu\nu}\left[x_1\left\{\left(h^2 - x_1^2\right)\mu - 6\eta\right\} + 6h\eta\,\mathrm{cosech}\left(h\sqrt{\frac{\mu}{\eta}}\right)\sinh\left(x_1\sqrt{\frac{\mu}{\eta}}\right)\right] \quad (12)$$

where $\nu(=\mu/\rho_0)$ is the kinematic viscosity and

Table 1
Order of base polynomial independency.

No. of grid points	N	$G = 1000,\ Pr = 6,\ \Lambda_c = 5,\ a = 1.5$		$G = 500,\ Pr = 10,\ \Lambda_c = 10,\ a = 0.5$	
		c_r	c_i	c_r	c_i
1501	5	−0.98451753	−20.77093642	−0.51541614	14.02106065
	10	−1.36292584	−20.81058032	−0.50446281	14.08347133
	15	−1.30325876	−20.77491326	−0.50330389	14.08103093
	20	−1.32266683	−20.77631900	−0.50370766	14.08202431
	25	−1.31257952	−20.77632666	−0.50360305	14.08203570
	30	−1.31268480	−20.77632916	−0.50362153	14.08203212
	35	−1.31268474	−20.77632906	−0.50362135	14.08203201
	40	−1.31268476	−20.77632902	−0.50362134	14.08203203
	50	−1.31268477	−20.77632904	−0.50362133	14.08203205
	60	−1.31268477	−20.77632903	−0.50362133	14.08203205
	70	−1.31268477	−20.77632904	−0.50362133	14.08203206

Table 2
Comparison of Galerkin and Chebyshev collocation method for different values of Pr and Λ_c.

Λ_c	Pr	Galerkin method			Chebyshev collocation method		
		G_c	a_c	c_c	G_c	a_c	c_c
0	1	992.056	1.404	0	992.529	1.404	0
	5	982.516	1.384	0	982.991	1.385	0
	10	983.456	1.383	0	983.553	1.383	0
	20	301.163	0.823	±9.283122	301.176	0.821	±9.292101
	50	138.408	1.110	±4.438623	138.427	1.110	±4.441947
10	1	1133.029	1.501	0	1133.178	1.501	0
	5	1119.363	1.483	0	1119.987	1.483	0
	10	1119.195	1.482	0	1119.195	1.482	0
	20	312.842	0.882	±9.482435	313.169	0.882	±9.487368
	50	160.731	1.12	±5.076330	161.001	1.121	±5.077923
20	1	1018.032	1.432	0	1018.423	1.432	0
	5	1006.577	1.412	0	1006.778	1.412	0
	10	1007.213	1.412	0	1007.299	1.413	0
	20	305.298	0.817	±9.227417	305.378	0.817	±9.231406
	50	145.106	1.108	±4.558382	145.193	1.109	±4.559101

$$p_b = \text{const} - \rho_0 g x_3 \tag{13}$$

4. Linear stability analysis

To study the linear stability of fluid flow, we superimpose an infinitesimal disturbance on the base flow in the form

$$u_i = W_b(x_1)\delta_{i3} + u_i', \quad p = p_b(x_3) + p', \quad T = T_b(x_1) + T', \quad \rho = \rho_b(x_1) + \rho' \tag{14}$$

According to the Squire theorem [21], the critical Grashof number can be obtained by considering two-dimensional disturbances rather than three dimensional disturbances. Substituting Eq. (14) into Eqs. (1), (5), and (6), linearising and restricting the attention to two-dimensional disturbances, we obtain

$$\frac{\partial u_1}{\partial x_1} + \frac{\partial u_3}{\partial x_3} = 0 \tag{15}$$

$$\frac{\partial u_1}{\partial t} + W_b \frac{\partial u_1}{\partial x_3} = -\frac{1}{\rho_0}\frac{\partial p}{\partial x_1} + \nu \nabla^2 u_1 - \frac{\eta}{\rho_0}\nabla^4 u_1 \tag{16}$$

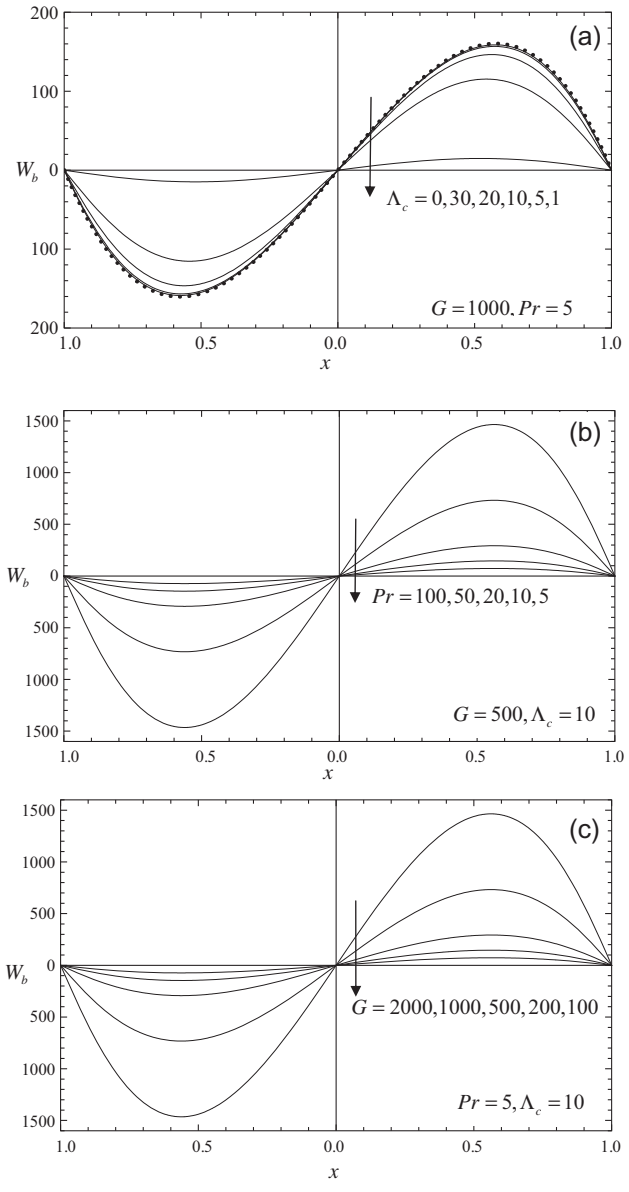

Fig. 2. Velocity profile of the base flow.

$$\frac{\partial u_3}{\partial t} + u_1 DW_b + W_b \frac{\partial u_3}{\partial x_3} = -\frac{1}{\rho_0}\frac{\partial p}{\partial x_3} + \nu \nabla^2 u_3 - \frac{\eta}{\rho_0}\nabla^4 u_3 + \alpha T g \tag{17}$$

$$\frac{\partial T}{\partial t} + W_b \frac{\partial T}{\partial x_3} + \frac{u_1}{2} = \kappa \nabla^2 T \tag{18}$$

where $D = d/dx_1$ and $\nabla^2 = \partial^2/\partial x_1^2 + \partial^2/\partial x_2^2$. Non-dimensionalizing Eqs. (15)–(18) by scaling (x_1, x_2, x_3) by h, t by h^2/ν, u_i by κ/h, T by βh and p by $\rho_0 \kappa \nu / h^2$, we get

$$\frac{\partial u_1}{\partial x_1} + \frac{\partial u_3}{\partial x_3} = 0 \tag{19}$$

$$\frac{\partial u_1}{\partial t} + \frac{W_b}{Pr}\frac{\partial u_1}{\partial x_3} = -\frac{\partial p}{\partial x_1} + \nabla^2 u_1 - \frac{1}{\Lambda_c^2}\nabla^4 u_1 \tag{20}$$

$$\frac{\partial u_3}{\partial t} + \frac{1}{Pr}\left(u_1 DW_b + W_b \frac{\partial u_3}{\partial x_3}\right) = -\frac{\partial p}{\partial x_3} + \nabla^2 u_3 - \frac{1}{\Lambda_c^2}\nabla^4 u_3 + GPrT \tag{21}$$

$$\frac{\partial T}{\partial t} + \frac{1}{Pr}\left(W_b \frac{\partial T}{\partial x_3} + \frac{u_1}{2}\right) = \frac{1}{Pr}\nabla^2 T \tag{22}$$

where, $Pr = \nu/\kappa$ is the Prandtl number, $G = \alpha g \beta h^4/\nu^2$ is the Grashof number, $\Lambda_c = h\sqrt{\mu/\eta}$ is the couple stress parameter. It should be noted here that the basic velocity in dimensionless form is

$$W_b = -\frac{GPr}{12\Lambda_c^2}\left[x_1\left\{6 + \Lambda_c^2(-1 + x_1^2)\right\} - 6\text{cosech}(\Lambda_c)\sinh(x_1\Lambda_c)\right] \tag{23}$$

Eliminate the pressure p from the momentum equation and introducing a stream function $\psi(x_1, x_3, t)$ through

Table 3
Variation of G_c, a_c and c_c as a function of Pr and Λ_c.

Λ_c	Pr	G_c	a_c	c_c
0	6.9	983.059	1.384	0
	7.0	983.077	1.384	0
	10.5	983.500	1.383	0
	10.6	983.508	1.383	0
	12.5	983.641	1.383	0
	12.6	983.646	1.383	0
	12.7	983.652	1.383	0
	12.8	826.162	0.399	±24.67603571
5	6.9	1862.857	1.585	0
	7.0	1589.04	0.427	±33.7676377
	10.5	702.359	0.759	±15.4107643
	10.6	694.164	0.765	±15.2389444
	12.5	577.913	0.844	±12.8195316
	12.6	573.289	0.845	±12.7263330
	12.7	568.787	0.848	±12.6327679
	12.8	564.389	0.851	±12.5412616
10	6.9	1119.261	1.483	0
	7.0	1119.257	1.483	0
	10.5	1119.19	1.482	0
	10.6	998.431	0.400	±27.13636194
	12.5	600.676	0.599	±16.53774459
	12.6	590.568	0.606	±16.26967541
	12.7	580.938	0.614	±16.01170690
	12.8	571.736	0.621	±15.76694478
30	6.9	992.794	1.396	0
	7.0	992.809	1.396	0
	10.5	993.177	1.396	0
	10.6	993.184	1.396	0
	12.5	993.301	1.395	0
	12.6	836.445	0.393	±24.77670377
	12.7	808.222	0.400	±23.97625617
	12.8	784.654	0.405	±23.31291980

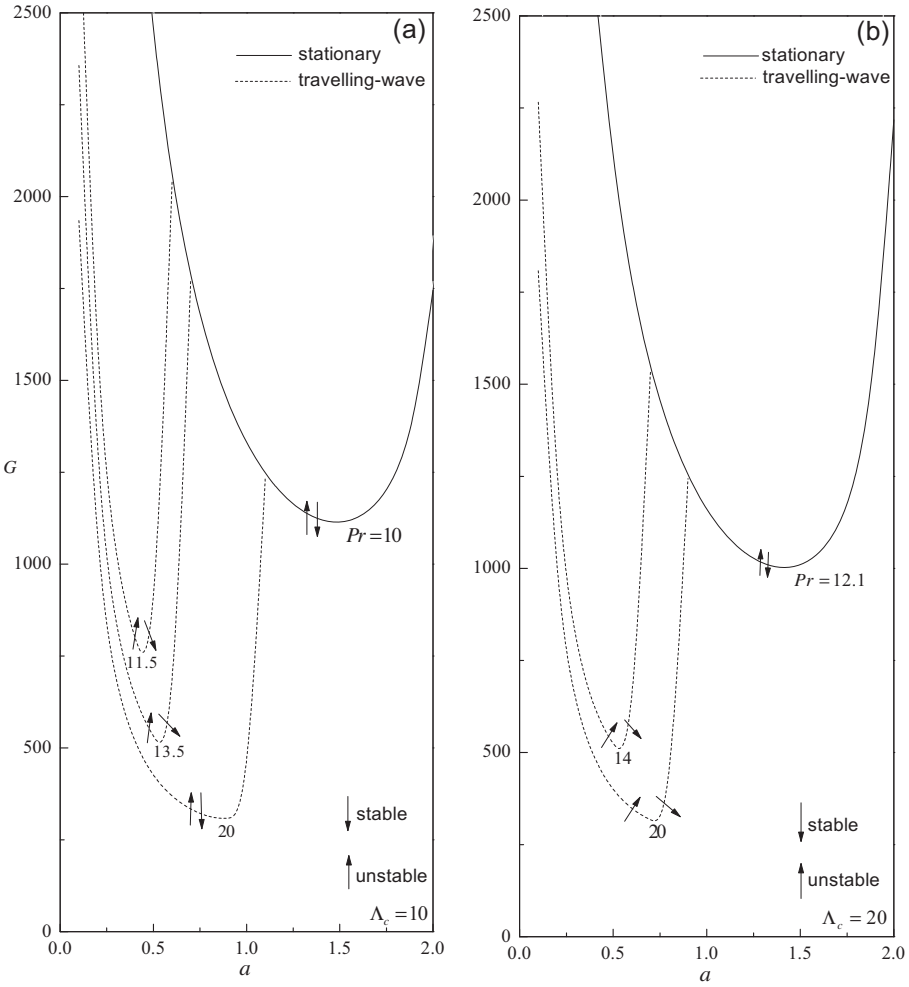

Fig. 3. Neutral stability curves.

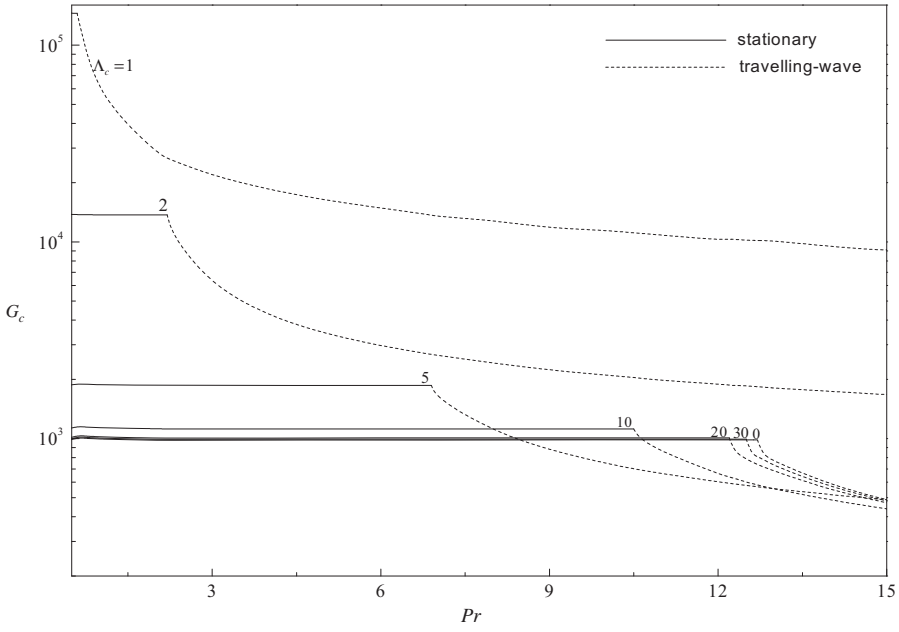

Fig. 4. Variation of the critical Grashof number G_c with the Prandtl number Pr for various values of Λ_c.

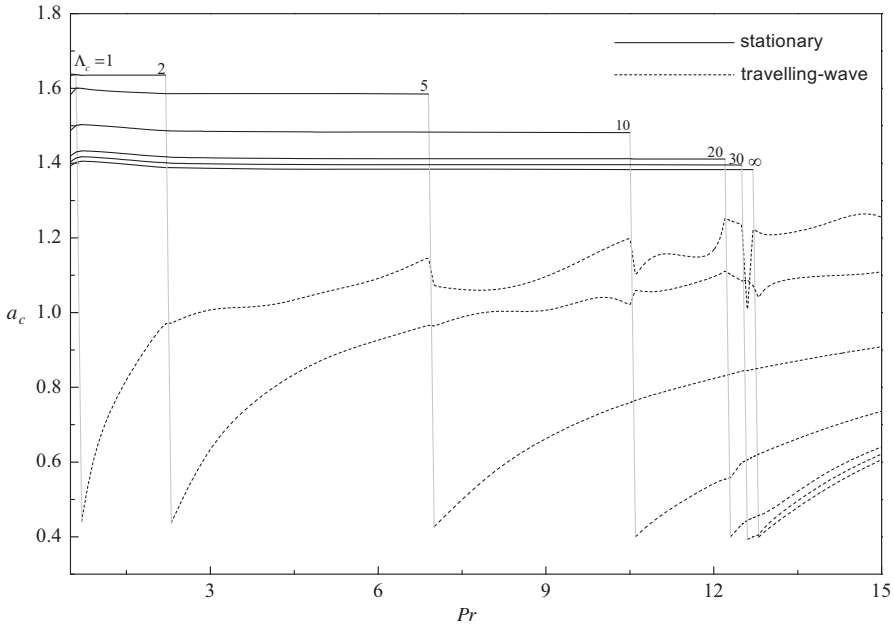

Fig. 5. Variation of the critical wave number a_c with the Prandtl number Pr for various values of Λ_c.

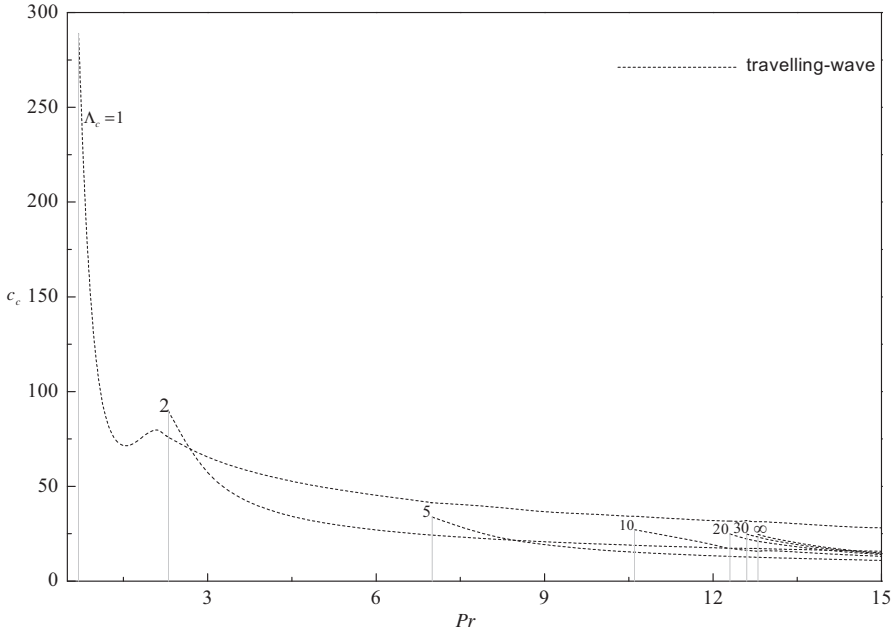

Fig. 6. Variation of the critical wave speed c_c with the Prandtl number Pr for various values of Λ_c.

$$u_1 = \frac{\partial \psi}{\partial x_3},\ u_3 = -\frac{\partial \psi}{\partial x_1} \tag{24}$$

and employing the normal mode analysis procedure in which we look for the solution of the form

$$\{\psi, T\}(x_1, x_3, t) = \{\Psi, \theta\}(x_1)\exp\left[ia(x_3 - ct)\right] \tag{25}$$

where c is the wave speed and a is the vertical wave number which is real and positive, we then obtain

$$\left(\frac{W_b}{Pr} - c\right)\left(D^2 - a^2\right)\Psi - \frac{1}{Pr}D^2 W_b \Psi = \frac{1}{ia}\left[\left(D^2 - a^2\right)^2 \Psi - \frac{1}{\Lambda_c^2}\left(D^2 - a^2\right)^3 \Psi - GPrD\theta\right] \tag{26}$$

$$\left(\frac{W_b}{Pr} - c\right)\theta + \frac{1}{2Pr}\Psi = \frac{1}{iaPr}\left(D^2 - a^2\right)\theta \tag{27}$$

In general, $c = c_r + ic_i$, where c_r is the phase velocity and c_i is the growth rate.

The associated boundary conditions are:

$$\Psi = D\Psi = D^3\Psi = \theta = 0 \text{ at } x_1 = \pm 1 \tag{28}$$

5. Numerical solution

Eqs. (26) and (27) together with the boundary conditions (28) constitute an eigenvalue problem which has to be solved numerically. The resulting eigenvalue problem is solved using Galerkin

method. Accordingly, $\Psi(x_1)$ and $\theta(x_1)$ are expanded in terms of Legendre polynomials in the form

$$\Psi(x_1) = \sum_{n=0}^{N} a_n \xi_n(x_1), \quad \theta(x_1) = \sum_{n=0}^{N} b_n \zeta_n(x_1) \tag{29}$$

with the corresponding base functions

$$\xi_n(x_1) = \left(x_1^2 - 3\right)\left(x_1^2 - 1\right)^2 P_n(x_1), \quad \zeta_n(x_1) = \left(1 - x_1^2\right) P_n(x_1)$$

where, $P_n(x_1)$ is the Legendre polynomial of degree n and a_n and b_n are constants. It may be noted that $\Psi(x_1)$ and $\theta(x_1)$ satisfies the boundary conditions. Eq. (29) is substituted into Eqs. (26) and (27) and the resulting error is required to be orthogonal to $\xi_m(x_1)$ and $\zeta_m(x_1)$ for $m = 0, 1, 2, \ldots N$. This gives

$$\begin{aligned}
&\frac{Pr}{\Lambda_c^2}\sum_{n=0}^{N} a_n \int_{-1}^{1} \left(\xi_n''' \xi_m''' + 3a^2 \xi_n'' \xi_m'' + 3a^4 \xi_n' \xi_m' + a^6 \xi_n \xi_m\right) dx_1 \\
&+ Pr \sum_{n=0}^{N} a_n \int_{-1}^{1} \left(\xi_n'' \xi_m'' + 2a^2 \xi_n' \xi_m' + a^4 \xi_n \xi_m\right) dx_1 \\
&+ ia \sum_{n=0}^{N} a_n \int_{-1}^{1} \left\{ \left(\frac{d^2 W_b}{dx_1^2} + a^2 W_b \right) \xi_n \xi_m - W_b \xi_n'' \xi_m \right\} dx_1 \\
&- GPr^2 \sum_{n=0}^{N} b_n \int_{-1}^{1} \zeta' \xi_m \, dx_1 = iac \, Pr \sum_{n=0}^{N} a_n \int_{-1}^{1} \left(\xi_n' \xi_m' + a^2 \xi_n \xi_m\right) dx_1
\end{aligned} \tag{30}$$

$$\begin{aligned}
&\frac{ia}{2}\sum_{n=0}^{N} a_n \int_{-1}^{1} \xi_n \zeta_m \, dx_1 + ia \sum_{n=0}^{N} b_n \int_{-1}^{1} W_b \, \zeta_n \zeta_m \, dx_1 \\
&+ \sum_{n=0}^{N} b_n \int_{-1}^{1} \left(\zeta_n' \zeta_m' + a^2 \zeta_n \zeta_m\right) dx_1 = iac \, Pr \sum_{n=0}^{N} b_n \int_{-1}^{1} \zeta_n \zeta_m \, dx_1
\end{aligned} \tag{31}$$

in which the primed quantities denote differentiation with respect to x_1.

The above equations form the following system of linear algebraic equations

$$AX = cBX \tag{32}$$

where A and B are the complex matrices, c is the eigenvalue and X is the eigenvector. To solve the above system (32), the DGVLCG of the IMSL library [22] is employed. The routine is based on the QZ algorithm due to Moler and Stewart [23]. The first step of this algorithm is to simultaneously reduce A to upper Heisenberg form and B to upper triangular form. Then, orthogonal transformations are used to reduce A to quasi-upper-triangular form while keeping B upper triangular. The generalised eigenvalues for the reduced problem are then computed as detailed below.

For fixed values of Pr, Λ_c, a and G, the values of c which ensure a non trivial solution of Eq. (32) can be obtained as the eigenvalues of the matrix $B^{-1}A$. From $2(N+1)$ eigenvalues $c(1), c(2), \ldots, c(2N+2)$, the one having the largest imaginary part ($c(p)$, say) is

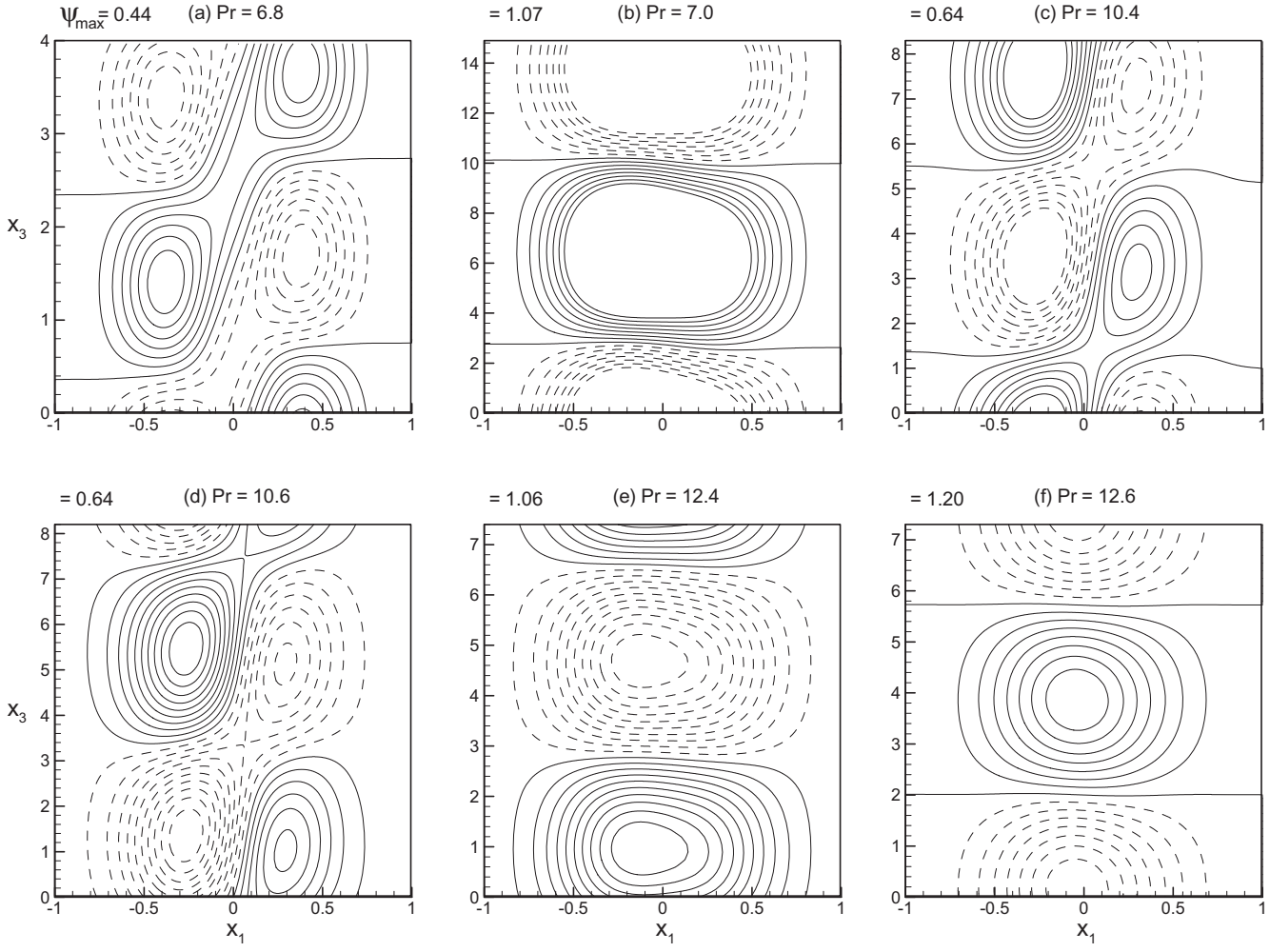

Fig. 7. Pattern variation of streamlines as a function of Pr for $\Lambda_c = 5$.

selected. In order to obtain the neutral stability curve, the value of G for which the imaginary part of $c(p)$ vanishes must be sought. Let this value of G be noted by G_q. The lowest point of G_q as a function of a gives the critical Grashof number G_c and the critical wave number a_c. The real part of $c(p)$ corresponding to G_c and a_c gives the critical wave speed c_c. If $c_c = 0$, the critical disturbance modes are stationary, whereas for $c_c \neq 0$ they are travelling waves. This procedure is repeated for various values of Pr and Λ_c.

6. Results and discussion

The effect of couple stresses on the stability of natural convection in a vertical fluid layer is investigated. The resulting eigenvalue problem of Orr–Sommerfeld type is solved numerically using higher order Galerkin technique with Legendre polynomials as trial functions and wave speed as the eigenvalue. The critical Grashof number and the critical wave speed are computed with respect to the wave number for various values of couple stress parameter and the Prandtl number.

The convergence of the numerical method employed is tested by varying the order of base polynomial. Table 1 illustrates the convergence of numerical solution as a function of order of polynomials for two different set of parameters. To account for all the harmonics in a complicated solution, a large number of terms have to be included in the expansion. We have chosen different orders of base polynomials and four digits point accuracy was achieved by retaining 31 terms in Eq. (29). As the number of terms increased in Eq. (29), the results were found to remain consistent and accuracy improved up to 7 digits for $N = 40$. By rigorous computational analysis, it was found that accurate solutions up to 8th digit could be reached by taking 50 terms in the Galerkin expansion and hence the results are obtained by taking $N = 50$. To know the accuracy of the numerical method employed to extract the stability parameters, the results are also obtained using Chebyshev collocation method (Appendix A) for a representative set of parametric values and compared in Table 2. From the Table it is seen that the results are in good agreement.

Fig. 2(a–c), respectively show the influence of couple stress parameter Λ_c, Prandtl number Pr and Grashof number G on the basic velocity profile W_b. These figures indicate that decrease in Λ_c, Pr and G is to suppress the fluid flow. From the figures, it is also seen that the solution does not have symmetry with respect to x_1, in general. This effect is due to the fixed direction of the gravitational field. The velocity profiles are antisymmetric about the vertical line at $x_1 = 0$ however, they are not precisely centrosymmetric about $x_1 = \pm 1/2$. In other words, in one half of the region, the basic flow is in one direction and in the other half it is in the opposite direction and is zero at $x_1 = 0$. Also, it is noticed from Fig. 2(a) that for $\Lambda_c = 30$, the solution is almost same as the non-polar solution (dotted line). For small values of Λ_c, that is for large couple stresses, the velocities are lower than that of non-polar case.

In Table 3, the critical Grashof number G_c, the critical wave number a_c and the critical wave speed c_c are tabulated for different values of Λ_c and Prandtl number Pr, as the magnitude of Pr

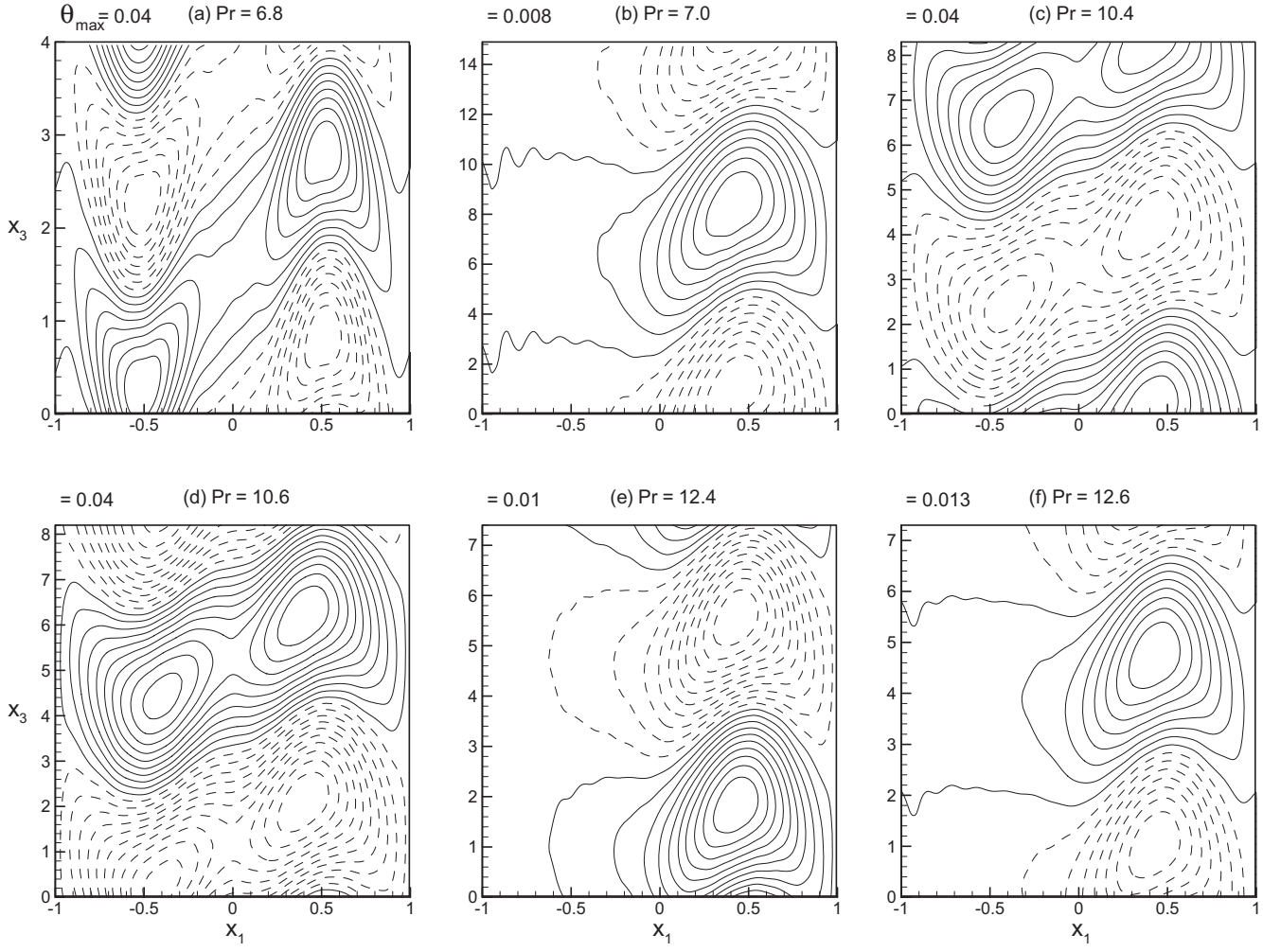

Fig. 8. Pattern variation of isotherms as a function of Pr for $\Lambda_c = 5$.

determines the mode of instability. When $\Lambda_c \neq 0$, the value of Pr at the point of intersection from stationary to travelling-wave mode is found to increase with increasing Λ_c. Besides, the critical Grashof number G_c at the transition mode decreases with increasing Λ_c. Moreover the value of Pr, at which the transition mode occurs, approaches to that of non-polar case as Λ_c increases. To justify our numerical results, test computations have been performed for $1/\Lambda_c = 0$ The critical Prandtl number at the transition between the stationary mode and travelling-wave mode predicted by the present code is 12.7, which is in agreement with the well established result in the literature (Korpela et al. [9], Bergholz [24]). We also find that as Pr increases, c_c decreases for all values of Λ_c considered in a manner similar to that of maximum base velocity. It is well known that the critical wave speed must be less than the maximum velocity of the base flow in the case of inviscid, homogeneous, parallel shear flows. The results presented in the tables also exhibit similar behaviour. This is to be expected, because the thermal disturbances tend to be heavily damped at high values of Pr.

The neutral stability curves in the (G, a) – plane are displayed in Fig. 3(a) and (b) for different values of Pr when $\Lambda_c = 10$ and 20, respectively. The neutral stability curves exhibit single but different minimum with respect to the wave number for various values of Λ_c and Pr. The portion below each neutral curve corresponds to a stable region and the region above corresponds to instability. It may be noted that, increase in Pr leads to decrease in the region of stability.

Figs. 4 and 5 illustrate the variation of critical Grashof number G_c and the corresponding critical wave number a_c as a function of Prandtl number Pr for different values of Λ_c. Depending on the value of Λ_c, there exists a threshold value of Pr at which the instability switches over from stationary to travelling-wave mode (Fig. 4). Moreover, the threshold value of Pr increases noticeably with increasing Λ_c. The results presented for $\Lambda_c \to \infty$ corresponds to non-polar fluids. In the stationary mode, increasing Λ_c is to decrease G_c and thus it has a destabilising effect on the system. In other words, increase in the couple stress viscosity stabilizes the flow against stationary mode. This is because the effect of suspended particles is to increase the viscosity of the fluid and thereby exhibits stabilizing influence on the system. However, Λ_c shows a dual behaviour on G_c if the instability is via travelling-wave mode. It is also seen from the figure that the dependence of G_c upon Pr is very weak in the case of stationary mode, while G_c for travelling-wave mode is a strongly decreasing function of Pr. The vertical lines represent the discontinuous changes in a_c due to the transition from stationary to travelling-wave mode (Fig. 5). It is evident from the figure that the dependence of a_c at stationary mode upon Pr is weak, whereas a_c at travelling-wave mode depends strongly upon Pr. Further it is seen that if the disturbances are stationary, the critical wave number decreases marginally with increasing Pr while it increases when the disturbances are travelling waves for a particular value of Λ_c. The same trend is observed for all values of Λ_c.

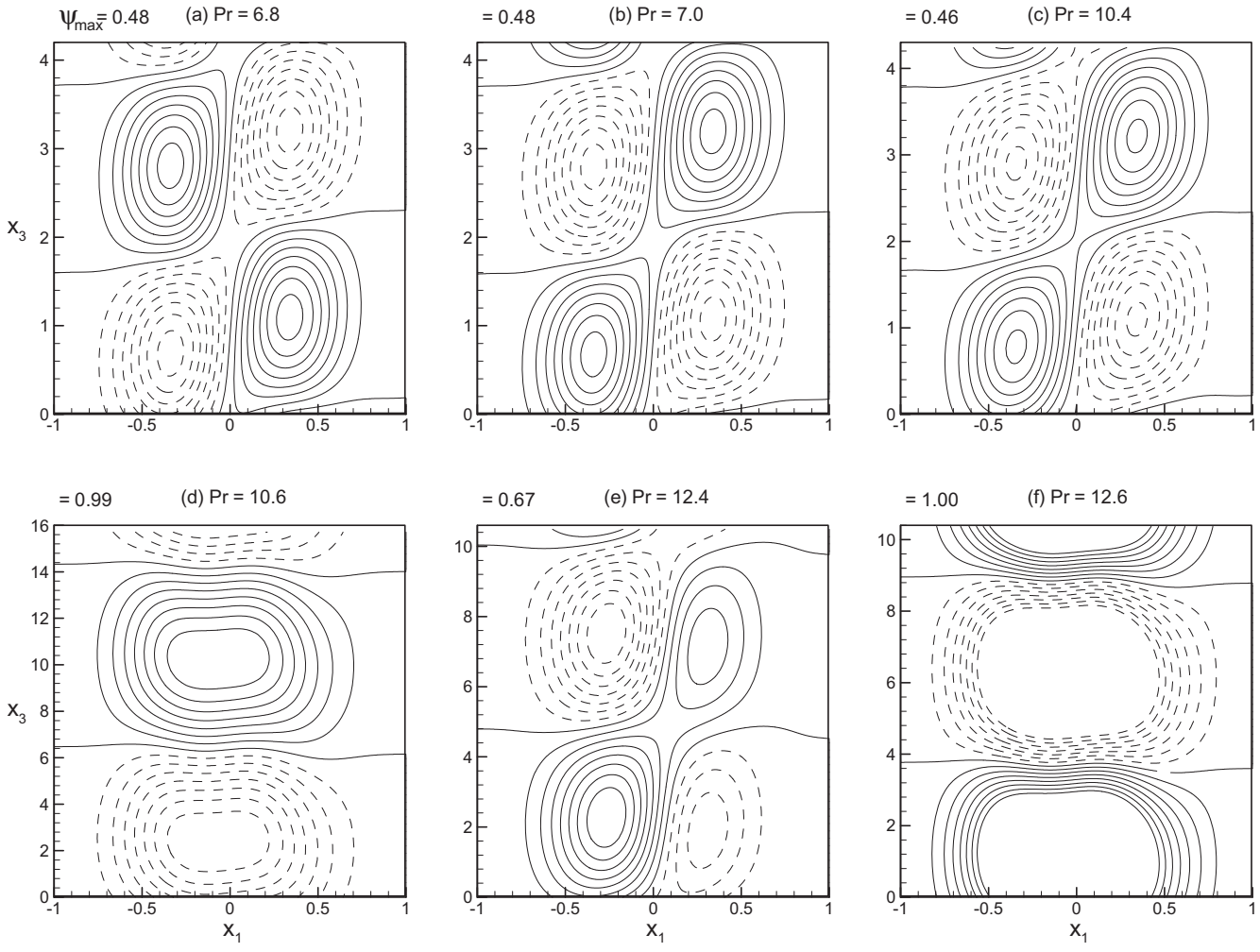

Fig. 9. Pattern variation of streamlines as a function of Pr for $\Lambda_c = 10$.

There is a weak dependence of G_c upon Pr in the case of stationary mode for all the values of Λ_c considered (Fig. 4). This may be due to the fact that energy for stationary instability at low to moderate Pr is derived mainly from the base flow velocity field through the action of disturbance Reynolds stresses at the mid-plane between the upward and the downward flowing convective streams. Also, it is observed that buoyancy forces work to enhance the instability when Λ_c is small and to retard it when Λ_c increases gradually.

A closer inspection of Fig. 5 reveals that, through the transition, the wave number drops suddenly with Pr for different values of Λ_c, and then increases again with further increase in the values of Pr. This indicates two different physical mechanisms of instability. As Pr increases, there is a tendency for more of the disturbance energy to originate from the potential energy associated with the buoyancy effect than as transfer from the kinetic energy of the base flow by the action of Reynolds stresses.

Additional information regarding the nature of the travelling-wave instability are summarised in Fig. 6, indeed confirm the above observed behaviour more evidently, which shows the variation of positive c_c with Pr for various values of Λ_c. The discontinuous changes in c_c due to the transition from stationary ($c_c = 0$) to travelling-wave ($c_c \neq 0$) mode are represented by the vertical lines. Fig. 6 demonstrates that c_c for the travelling-wave mode is a decreasing function of both Pr and Λ_c.

To have a thorough understanding about the stability behaviour of the fluid flow in the above discussed case, streamlines and isotherms at the critical state for both stationary and travelling-wave modes are analyzed. Figs. 7 and 8 show the results for different values of Pr and a particular value of $\Lambda_c = 5$. In the figures, dotted and solid lines represent negative and positive values, respectively. For $Pr = 6.8$, the flow pattern appears to be stationary and bicellular. Further, the streamlines move closer and become parallel at the centre of the vertical fluid layer (Fig. 7(a)). The isotherms are bicellular oblate triangles which are occupying almost the whole thickness of vertical fluid layer and the same is evident from Fig. 8(a). The flow pattern and flow strength changes qualitatively as well as quantitatively as the mode changes from stationary to travelling-wave with increasing Prandtl number. In other words, the instability switches over from stationary to travelling-wave mode once the value of Pr exceeds the value 6.9. When $Pr = 7$, convective cells transform into unicellular form bicellular in streamlines (Fig. 7(b)). Also, shapes of the isotherms changes from bicellular oblate triangles to unicellular oblate triangles and concentrate in the vicinity of the hot wall (Fig. 8(b)). It is further seen that the actual wavelengths are substantially larger in both streamlines and isotherms and at this stage ψ_{max} increases from 0.44 to 1.07, also θ_{max} changes from 0.04 to 0.008. This fact is also evident from Figs. 7 and 8(b). Further increase in Pr is to decrease the flow strength (Fig. 7(e) and (f)) and also to weaken the isotherms

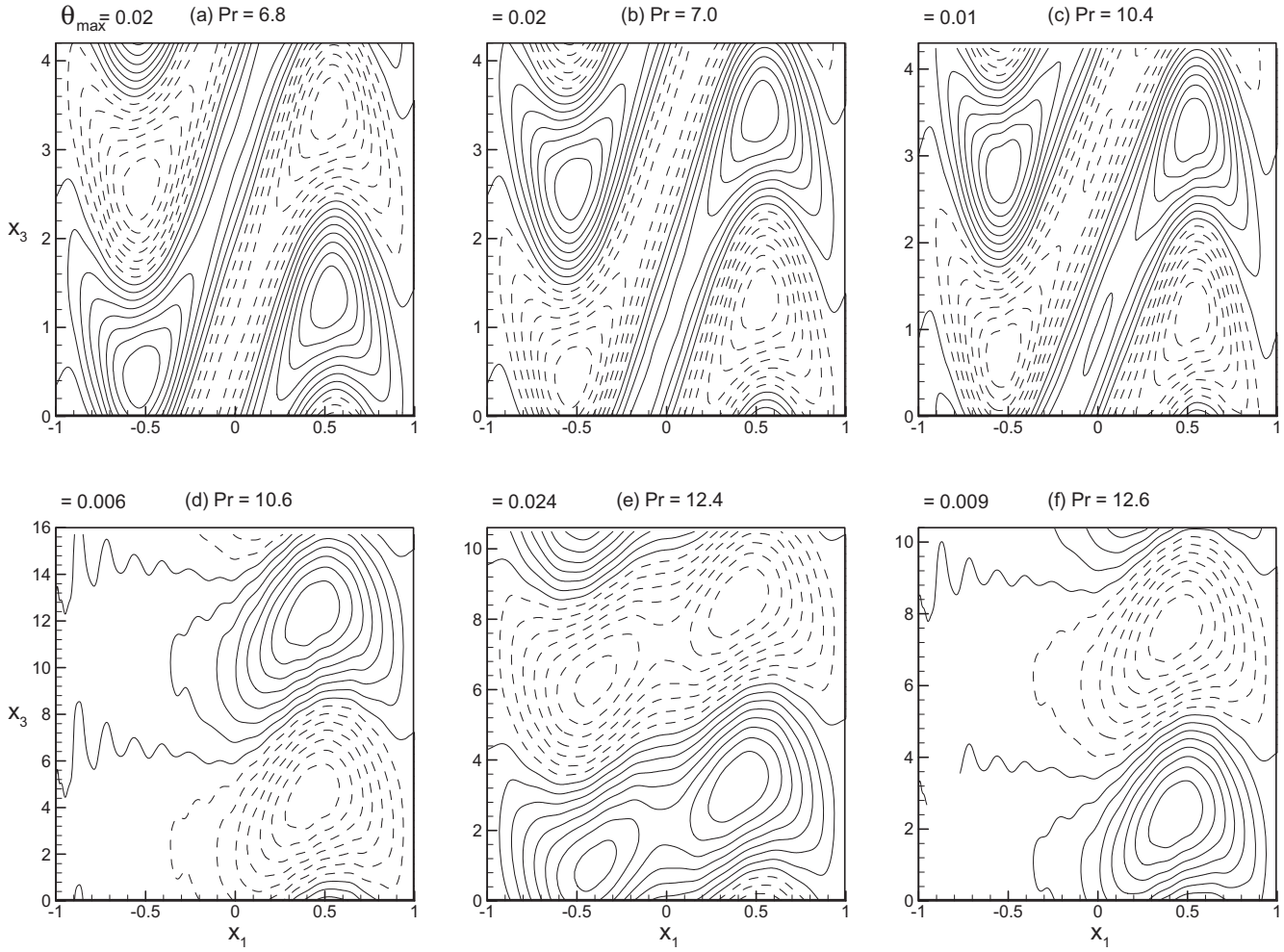

Fig. 10. Pattern variation of isotherms as a function of Pr for $\Lambda_c = 10$.

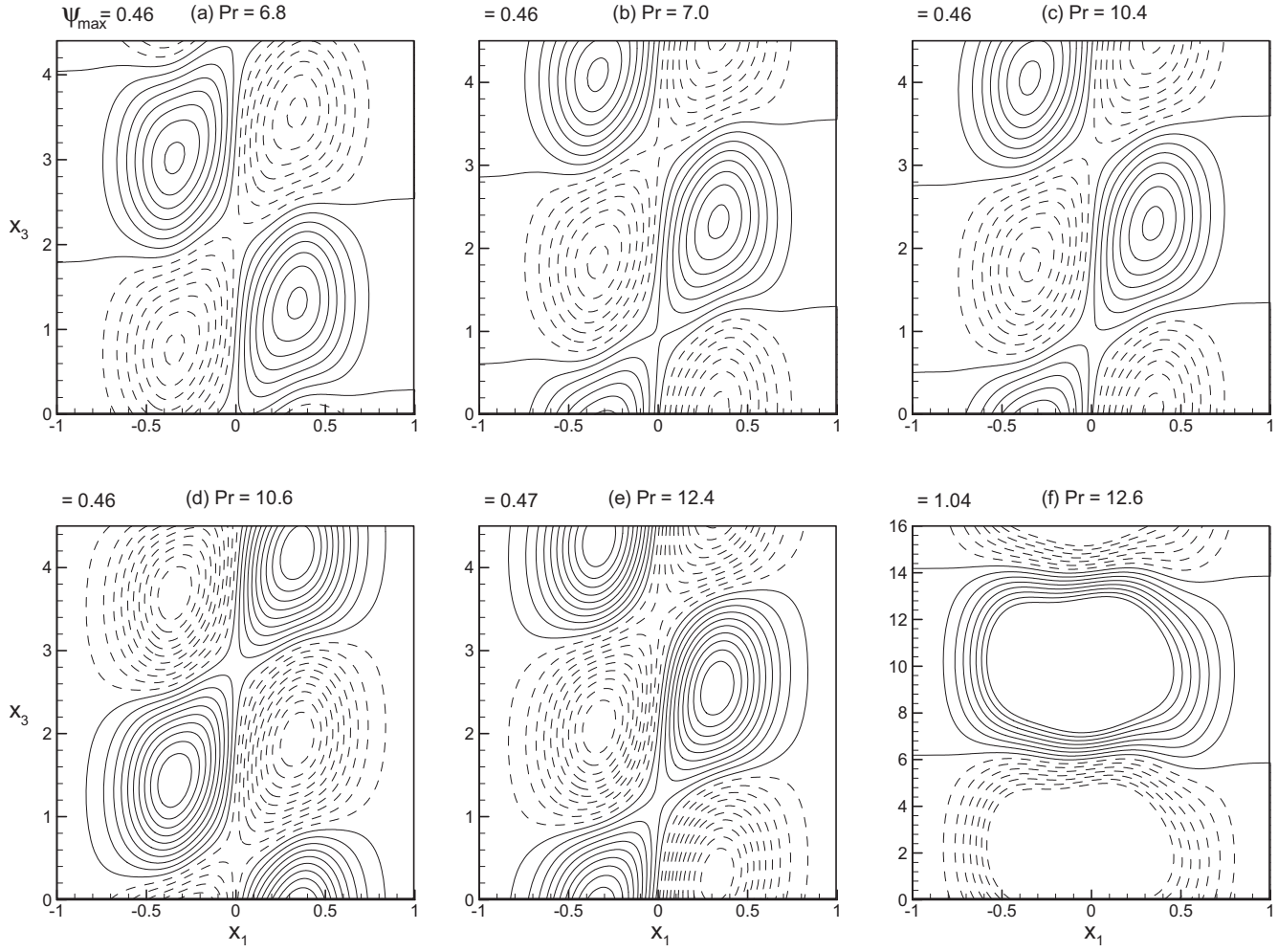

Fig. 11. Pattern variation of streamlines as a function of *Pr* for $\Lambda_c = 30$.

(Fig. 8(e) and (f)). From these figures, it is also observed that the cells change from unicellular to bicellular in streamlines and oblate triangles to bicellular with an inclination. With increasing *Pr* further, the streamline and isotherm patterns appear to be same as those observed for value of *Pr* at which the transition mode took place. However, the wavelength is found to be decreasing with increasing *Pr*.

To study the effect of couple stress parameter, results are presented for $\Lambda_c = 10$. The streamlines and isotherms are shown in Figs. 9 and 10(a–c), respectively for *Pr* = 6.8, 7.0 and 10.4. The pattern appears to be stationary bicellular convection in streamlines, whereas in isotherms bicellular oblate triangles. It is also observed that the magnitude of secondary flow is very weak. As *Pr* increases to 10.6 (Fig. 9(d)), a sudden change in the magnitude of secondary flow is observed (i.e., $\psi_{max} = 0.46–0.99$) and convective cell becomes unicellular. In the case of isotherms, as mode changes from stationary to oscillatory, the magnitude of isothermal lines reduces drastically ($\theta_{max} = 0.01–0.006$) and pattern variation is also observed (Fig. 10(d)). This behaviour of the streamlines and isotherms may be due to the change in the mode of instability from stationary to travelling-wave mode. It amounts to change in the streamline pattern from unicellular to bicellular and again to unicellular as observed from Fig. 9(e) and (f) with increase in the value of *Pr*. A change in the isotherm patterns is also observed from oblate triangles to bicellular with an inclination and then to oblate triangles (Fig. 10(e) and (f)).

Figs. 11 and 12 exhibit the evolution of profile patterns before and after the transition mode as a function of *Pr* for $\Lambda_c = 30$. We observe almost the same pattern for *Pr* = 6.8, 7.0, 10.4, 10.6 and 12.4 in both streamlines and isotherms (Figs. 11 and 12(a–e)). Figs. 11 and 12(f) illustrate the results for *Pr* = 12.6. From these figures, it is observed that the flow strength suddenly changes both qualitatively and quantitatively in both streamlines and isotherms. Also, there is a sudden increase in wavelength and this confirms that transition mode occurs at this point.

7. Conclusions

The stability of natural convection of a vertical couple stress fluid layer is studied using linear stability theory. An eigenvalue problem of Orr–Sommerfeld type is solved using the Galerkin method with Legendre polynomials as trial functions. The critical Grashof number G_c, the critical wave number a_c and the critical wave speed c_c are computed for wide ranges of couple stress parameter Λ_c and the Prandtl number *Pr*. The couple stress parameter Λ_c shows destabilising effect on the system at the stationary mode. To the contrary, it exhibits a dual behaviour once the instability is via travelling-wave mode. Moreover, the value of *Pr* increases at which transition from stationary to travelling-wave instability occurs as the value of Λ_c increases. The streamlines and isotherms are found to mimic the behaviour of stability curves

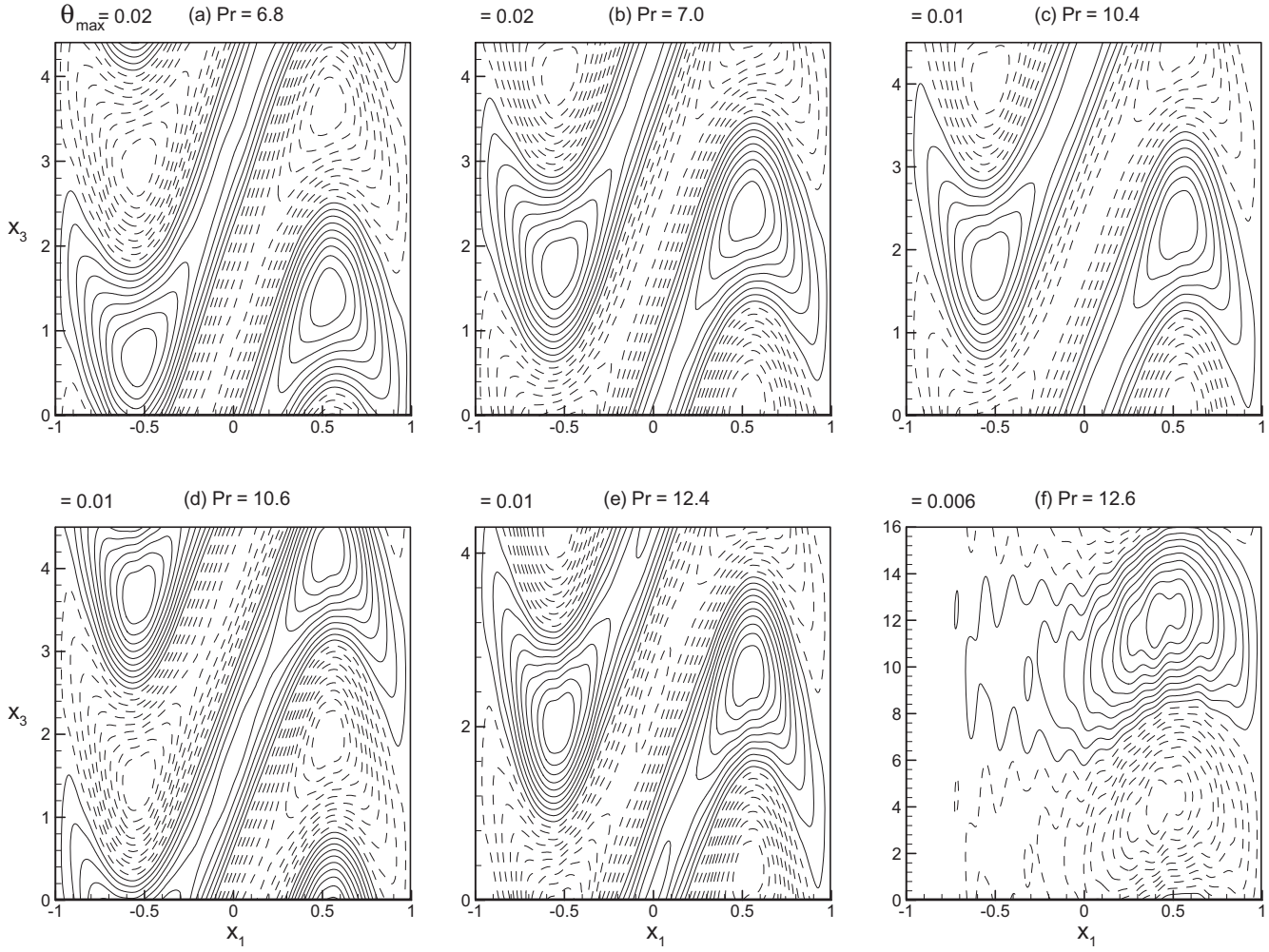

Fig. 12. Pattern variation of isotherms as a function of *Pr* for $\Lambda_c = 30$.

observed before and after the change of mode of instability. Besides, a sudden change in streamlines and isotherms is observed both in their magnitude and pattern just before and after the transition mode. For the range of parametric values considered, convective cells are found to appear both bicellular as well as unicellular in nature.

Conflict of interest

None declared.

Acknowledgments

The authors wish to thank the reviewers for their constructive comments and suggestions which were helpful in improving the quality of the paper. The authors are also thankful to Prof. N. Rudraiah for his valuable discussions. The author B.M.S wishes to thank the Head of the Department of Science and Humanities, Principal and the Management of the college for their encouragement and support.

Appendix A

The eigenvalue problem has also been solved using Chebyshev collocation method. The *k*th order Chebyshev polynomial is given by

$$\xi_k(x) = \cos k\theta,\ \theta = \cos^{-1} x \tag{A1}$$

The Chebyshev collocation points are given by

$$x_j = \cos\left(\frac{\pi j}{N}\right),\quad j = 0(1)N \tag{A2}$$

Here, the right and left wall boundaries correspond to $j = 0$ and N, respectively. The field variable Ψ and θ can be approximated in terms of Chebyshev variable as follows

$$\Psi(x) = \sum_{j=0}^{N} \xi_n(x_j)\Psi_j,\quad \theta(x) = \sum_{j=0}^{N} \xi_n(x_j)\theta_j \tag{A3}$$

The governing equations (26)–(28) are discretized in terms of Chebyshev variable x to get

$$\begin{aligned}
&\left(\frac{W_b}{Pr} - c\right)\left(\sum_{k=0}^{N} B_{jk}\Psi_k - a^2\Psi_j\right) - \frac{1}{Pr} D^2 W_b \Psi_j \\
&= \frac{1}{ia}\left(\sum_{k=0}^{N} D_{jk}\Psi_k - 2a^2\sum_{k=0}^{N} B_{jk}\Psi_k + a^4\Psi_j\right) \\
&\quad - \frac{1}{ia\Lambda_c^2}\left(\sum_{k=0}^{N} E_{jk}\Psi_k - 3a^2\sum_{k=0}^{N} D_{jk}\Psi_k + 3a^4\sum_{k=0}^{N} B_{jk}\Psi_k - a^6\Psi_j\right) \\
&\quad - \frac{GPr}{ia}\sum_{k=0}^{N} A_{jk}\theta_k,\quad j = 1(1)N-1
\end{aligned} \tag{A4}$$

$$\left(\frac{W_b}{Pr}-c\right)\theta_j+\frac{1}{2Pr}\Psi_j=\frac{1}{iaPr}\left(\sum_{k=0}^{N}B_{jk}\theta_k-\alpha^2\theta_j\right),\quad j=1(1)N-1 \tag{A5}$$

$$\Psi_0=\Psi_N=0 \tag{A6}$$

$$\sum_{k=0}^{N}A_{jk}\Psi_k=0,\quad j=0\ \&\ N \tag{A7}$$

$$\sum_{k=0}^{N}C_{jk}\Psi_k=0,\quad j=0\ \&\ N \tag{A8}$$

$$\theta_0=\theta_N=0 \tag{A9}$$

where

$$A_{jk}=\begin{cases}\frac{c_j(-1)^{k+j}}{c_k\left(x_j-x_k\right)} & j\neq k\\ \frac{x_j}{2\left(1-x_j^2\right)} & 1\leqslant j=k\leqslant N-1\\ \frac{2N^2+1}{6} & j=k=0\\ -\frac{2N^2+1}{6} & j=k=N\end{cases} \tag{A10}$$

$$B_{jk}=A_{jm}\cdot A_{mk},\ C_{jk}=B_{jm}\cdot A_{mk},\ D_{jk}=B_{jm}\cdot B_{mk}\ \&\ E_{jk}=D_{jm}\cdot B_{mk} \tag{A11}$$

with

$$c_j=\begin{cases}2 & j=0,N\\ 1 & 1\leqslant j\leqslant N-1\end{cases}$$

The above equations form the following system of linear algebraic equations

$$AX=cBX$$

References

[1] G.Z. Gershuni, On the stability of plane convective motion of a liquid, Zh. Tekh. Fiz. 23 (1953) 1838–1844.

[2] R.V. Birikh, On small perturbations of a plane parallel flow with cubic velocity profile, Prikl. Mat. Mekh. 30 (1966) 356–361. , Appl. Math. Mech. 30 (1966) 432–438.

[3] R.N. Rudakov, On small perturbations of convective motion between vertical parallel planes, Prikl. Mat. Mekh. 30 (1966) 362–368. , Appl. Math. Mech. 30 (1966) 439–445.

[4] K. Gotoh, M. Satoh, The stability of a natural convection between two parallel vertical planes, J. Phys. Soc. Jpn. 21 (1966) 542–548.

[5] R.N. Rudakov, Spectrum of perturbations and stability of convective motion between vertical planes, Prikl. Mat. Mekh. 31 (1967) 349–355. , Appl. Math. Mech. 31 (1967) 376–383.

[6] C.M. Vest, V.S. Arpaci, Stability of natural convection in a vertical slot, J. Fluid Mech. 36 (1969) 1–15.

[7] K. Gotoh, N. Ikeda, Asymptotic solution of the instability problem of channel flows with antisymmetric velocity profile, J. Phys. Soc. Jpn. 32 (1972) 845–850.

[8] R.V. Birikh, G.Z. Gershuni, E.M. Zhukhovitskii, R.N. Rudakov, On oscillatory instability of plane-parallel convective motion in a vertical channel, Prikl. Mat. Mekh. 36 (1972) 745–748. , Appl. Math. Mech. 36 (1972) 707–710.

[9] S.A. Korpela, D. Gozum, C.B. Baxi, On the stability of the conduction regime of natural convection in a vertical slot, Int. J. Heat Mass Transfer 16 (1973) 1683–1690.

[10] A.C. Eringen, Theory of micropolar fluids, J. Math. Mech. 16 (1966) 1–18.

[11] V.K. Stokes, Couple stresses in fluids, Phys. Fluids 9 (1966) 1709–1715.

[12] D. Gozum, V.S. Arpaci, Natural convection of viscoelastic fluids in a vertical slot, J. Fluid Mech. 64 (1974) 439–448.

[13] M. Takashima, The stability of natural convection in a vertical layer of viscoelastic liquid, Fluid Dyn. Res. 11 (1993) 139–152.

[14] J.K. Jain, V.K. Stokes, Effects of couple stresses on the stability of plane Poiseuille flow, Phys. Fluids 15 (1972) 977–980.

[15] M.S. Malashetty, S.N. Gaikwad, Mahantesh Swamy, An analytical study of linear and non-linear double diffusive convection with Soret effect in couple stress liquids, Int. J. Therm. Sci. 45 (2006) 897–907.

[16] S.N. Gaikwad, M.S. Malashetty, K. Ramaprasad, An analytical study of linear and non-linear double diffusive convection with Soret and Dufour effects in couple stress liquids, Int. J. Nonlinear Mech. 42 (2007) 903–913.

[17] Sunil, R. Devi, A. Mahajan, Global stability for thermal convection in a couple-stress fluid, Int. Commun. Heat Mass Transfer 38 (2011) 938–942.

[18] I.S. Shivakumara, M. Akkanagamma, C.O. Ng, Electrohydrodynamic instability of a rotating couple stress dielectric fluid layer, Int. J. Heat Mass Transfer 62 (2013) 761–771.

[19] I.S. Shivakumara, S.B. Naveen Kumar, Linear and weakly nonlinear triple diffusive convection in a couple stress fluid layer, Int. J. Heat Mass Transfer 68 (2014). 542-533.

[20] N. Rudraiah, B.M. Shankar, C.O. Ng, Electrohydrodynamic stability of couple stress fluid flow in a channel occupied by a porous medium, Special Topics Rev. Porous Med. 2 (2011) 11–22.

[21] P.G. Drazin, W.H. Reid, Hydrodynamic Stability, Cambridge University Press, Cambridge, UK, 2004.

[22] IMSL, International Mathematical and Statistical Library, 1982.

[23] C.B. Moler, G.W. Stewart, An algorithm for generalized matrix eigenvalue problems, SIAM (Soc. Ind. Appl. Math.) J. Numer. Anal. 10 (1973) 241–256.

[24] R.F. Bergholz, Instability of steady natural convection in a vertical fluid layer, J. Fluid Mech. 84 (1978) 743–768.